The Astrophysical Journal Letters, 874:L1 (6pp), 2019 March 20 https://doi.org/10.3847/2041-8213/ab0c9f

Properties of Slow Magnetoacoustic Oscillations of Solar Coronal Loops by Multi-instrumental Observations

V. M. Nakariakov[1,2], M. K. Kosak[1], D. Y. Kolotkov[1], S. A. Anfinogentov[3], P. Kumar[4], and Y.-J. Moon[2]
[1] Centre for Fusion, Space & Astrophysics, Physics Department, University of Warwick, Coventry CV4 7AL, UK; V.Nakariakov@warwick.ac.uk
[2] School of Space Research, Kyung Hee University, Yongin 17104, Republic of Korea
[3] Institute of Solar-Terrestrial Physics SB RAS, Lermontov St. 126, Irkutsk 664033, Russia
[4] Heliophysics Science Division, NASA Goddard Space Flight Center, Greenbelt, MD 20771, USA
Received 2018 July 26; revised 2019 March 3; accepted 2019 March 4; published 2019 March 19

Abstract

Rapidly decaying oscillations of the thermal emission detected in the decay phase of solar and stellar flares are usually interpreted as standing or sloshing (reflecting) slow magnetoacoustic oscillations. We determine the scalings of the oscillation periods, damping times, and amplitudes with the temperature, considering both standing and sloshing oscillations detected with different instruments. In addition, the time evolution of different spatial harmonics of a sloshing oscillation is considered. Parameters of slow oscillations observed in the EUV, X-ray, and microwave bands, and published in the literature, are used. The damping time of slow oscillations is found to scale almost linearly with the oscillation period, as the period to 0.87 ± 0.1, giving the average Q-factor determined as the ratio of the damping time to the period, of about 1. The Q-factor is found to scale with the relative amplitude to the power of $0.33^{+0.10}_{-0.11}$ with 95% confidence. The amplitudes of different spatial harmonics forming a sloshing pulse show similar time evolution, suggesting that the period-dependent dissipation is counteracted by another mechanism. The results obtained indicate that the damping of slow oscillations depends on the oscillation amplitude, and that the competition of nonlinear and dissipative effects could allow for the existence of wave pulses of a sustained shape.

Key words: magnetohydrodynamics (MHD) – Sun: corona – Sun: oscillations

1. Introduction

Slow magnetoacoustic oscillations of solar coronal loops, also often called "SUMER" oscillations, as they were discovered as periodic variations of the Doppler shift of hot emission lines with the high-resolution imaging spectrometer *Solar and Heliospheric Observatory* (*SOHO*)/SUMER (e.g., Wang et al. 2002) remain a popular research topic. In particular, the interest in SUMER oscillations is connected with the seismological estimation of the plasma-β and magnetic field in oscillating loops (Wang et al. 2007), and possible diagnostics of the coronal heating function (Nakariakov et al. 2017). Properties of SUMER oscillations may indicate the suppression of thermal conduction along the field (Wang et al. 2015, 2018). There is also a growing interest in the possible association of several-minute quasi-periodic pulsations detected in stellar flares with slow oscillations (see, e.g., Van Doorsselaere et al. 2016; McLaughlin et al. 2018, for recent reviews), which would provide us with the solid basis for the exploitation of the solar-stellar analogy (Cho et al. 2016; Kolotkov et al. 2018).

SUMER oscillations of coronal loops are characterized by relatively long periods, from a few minutes to a few tens of minutes, which correspond to the acoustic travel time along the oscillating loop; a very rapid damping, with a ratio of the damping time to the oscillation period of about unity; and a large relative amplitude that is more than 10% of the local sound speed (see Wang 2011, for a comprehensive review). The damping time of SUMER oscillations is found to scale linearly with the oscillation period (Wang et al. 2003; Mariska 2006). The quarter-period phase lag between velocity and intensity disturbances, detected in some cases (e.g., Wang et al. 2002), unequivocally indicate that SUMER oscillations are produced by a standing slow wave, at least in those cases.

Oscillatory phenomena similar to SUMER oscillations, have been observed with several other instruments. Mariska (2005, 2006) detected decaying oscillations in Doppler shifts in the S XV and Ca XIX emission lines observed with Yohkoh/BCS. The quarter-period phase shift between the Doppler-shift and intensity oscillations was detected in some cases, similar to that detected with SUMER. Mariska et al. (2008) studied a 35 minute Doppler shift oscillation in the Fe XII–Fe XV emission lines with *Hinode*/EIS. The oscillations in the lower temperature lines rapidly decayed, while the oscillation in Fe XV showed no evidence for decay. Despite the decayless behavior and the relatively low amplitude, of about 1% of the sound speed, the oscillation was interpreted as a standing slow mode. Srivastava & Dwivedi (2010) observed several-minute periodicities of intensity oscillations of Fe XII with *Hinode*/EIS, interpreted as the superposition of the fundamental and second harmonics of the slow mode. Reznikova & Shibasaki (2011) observed periodic variations of the microwave emission, with period growing from 2.5 to 5 minutes, with NoRH. Kim et al. (2012) detected decaying 13 minute intensity oscillations simultaneously in EUV and microwave, with *SDO*/AIA and NoRH, respectively. Kupriyanova et al. (2014) interpreted 2 minute pulsations of the thermal microwave emission detected with NoRH, as slow oscillations. The pulsations occur to be cophased along the entire emitting loop, as expected in the fundamental standing harmonic. Kupriyanova & Ratcliffe (2016) found damped one-minute oscillations of the microwave and X-ray emission during the decay phase of a flare, and interpreted it as a fundamental slow mode. Li et al. (2017) studied 10 minute oscillations in the Doppler shift and integrated intensity of the Fe XXI emission line observed with

IRIS, the soft X-ray flux measured with *GOES*, and EUV light curves obtained with *SDO*/AIA.

On the other hand, Kumar et al. (2013) observed a traveling intensity perturbation of a hot, 8–10 MK, coronal loop, in a C7.4 class flare, with *SDO*/AIA. The intensity variation was seen to bounce approximately four times between the loop's footpoints, before fading, i.e., exhibiting a "zigzag" pattern in a time–distance plot made along the apparent direction of the magnetic field. The oscillation period and decay time were about 630 s and 440 s, respectively. The apparent phase speed was about 460–510 km s^{-1} which matched the sound speed in the loop. The authors suggested calling this phenomenon a reflecting longitudinal wave, while Reale (2016) introduced the term "sloshing" oscillations for this phenomenon. A similar, bouncing back and forth between the footpoints, EUV intensity perturbation was detected in another C-class flare by Kumar et al. (2015). The period of the oscillation and decay time were about 409 s and 1121 s, respectively. The characteristic phase speed of the wave is about 560 km s^{-1}, which was roughly consistent with the sound speed at the temperature of about 10–16 MK. Wang et al. (2015) observed a clear sloshing pattern in the 131 Å intensity oscillation with *SDO*/AIA. The oscillation period, decay time, and the apparent phase speed were estimated as about 12 minutes, 9 minutes, and 500 km s^{-1}, respectively. Mandal et al. (2016) reported a simultaneous observation of a propagating and reflecting intensity disturbance in a hot coronal loop observed in EUV and X-rays with *SDO*/AIA and *Hinode*/XRT, respectively. In addition, three other cases of intensity pulses sloshing between footpoints were analyzed. In all considered cases the projected traveling speed was found to be lower than the local sound speed, consistent with the slow wave interpretation. Pant et al. (2017) observed antiphase oscillations of the 171 and 193 Å intensity oscillations at two ends of a nonflaring fan loop system observed with *SDO*/AIA. The oscillation period was estimated to be 27 minutes, the damping time of 45 minutes, and the apparent phase speed of about 75 km s^{-1}. The time–distance map made along the loop showed a sloshing (i.e., "zigzagging") motion pattern. We need to point out that sloshing oscillations are different from other manifestations of slow waves in the corona, propagating (not reflecting) slow waves that are detected in polar plumes and near footpoints of long loops (see, e.g., de Moortel 2009).

Numerical modeling of slow oscillations in a coronal loop reproduced main properties of standing (SUMER) and sloshing oscillations, i.e., the observed oscillation period, $P_{\rm slow} \approx 2L/C_{\rm s}$, where L is the loop length and $C_{\rm s}$ is the sound speed; and associated the rapid damping of the oscillation with the effect of thermal conduction (Ofman & Wang 2002). Nakariakov & Zimovets (2011) demonstrated that a similar periodicity could occur in arcades. The preferential excitation of lower, i.e., the fundamental and second parallel harmonics by an impulsive source, was found in, e.g., Nakariakov et al. (2004), Tsiklauri et al. (2004), and Taroyan et al. (2005). Effects of the loop curvature were shown to be weak (e.g., Selwa et al. 2007; Ogrodowczyk et al. 2009). The misbalance of the radiative losses and unspecified background coronal heating was found to significantly affect the oscillation quality factor (Nakariakov et al. 2017). Finite amplitude effects were shown to result in steepening of the oscillation and increasing the damping (e.g., Verwichte et al. 2008; Ruderman 2013; Kumar et al. 2016). Yuan et al. (2015) performed forward modeling of the manifestation of a slow mode of a hot coronal loop in the *SDO*/AIA and *SOHO*/SUMER data. Fang et al. (2015) reproduced numerically the phenomenon of a reflecting longitudinal wave in a hot coronal loop in the form of a plasma blob, and synthesized its manifestation in a spectral line. Reale et al. (2018) modeled sloshing oscillations in an extremely long magnetic tube connecting an Orion pre-main-sequence star with the surrounding disk. Recently, Wang et al. (2018) performed 1D numerical simulations of sloshing oscillations in a hot coronal loop, and concluded that quick formation of the fundamental standing mode following initially sloshing oscillations could be caused by enhanced compressive viscosity. However, a detailed study of the preferential excitation of either standing or sloshing oscillations has not been performed. Also, the reason why slow oscillations of both kinds are usually detected in the hot plasma emission remains unclear.

Both standing and sloshing oscillations are considered to be associated with the slow magnetoacoustic mode. Both these kinds of slow oscillations occur in closed magnetic configurations. Thus, one difference between SUMER and sloshing oscillations is the phase shift between the parallel velocity and density oscillations. In standing slow oscillations, the velocity and density perturbations are phase shifted by a quarter-period, while in the sloshing oscillations these perturbations are either in phase or in antiphase. This difference is not connected with the structure of the perturbation along the loop, i.e., with the number of parallel harmonics, which composes the perturbation. It is likely that at least some cases of SUMER oscillations could actually belong to the sloshing oscillation class. It is clear that the oscillations could be produced by any perturbation of the plasma pressure or a field-aligned flow, localized either in the loop or at its footpoints, provided the characteristic time of the perturbation is shorter than the acoustic travel time along the loop. Thus, the driver could be a rapid chromospheric or coronal heating event, a jet, or thermal overstability. But, in many events such impulsive energy depositions were not observed.

In this Letter we perform statistical analysis of slow oscillations of both SUMER and sloshing type, investigating the relationship between the oscillation periods, damping time, apparent amplitude, and sound speed; and compare the results with properties of sloshing oscillations.

2. Scalings of Slow Oscillation Parameters

We perform a statistical analysis of the slow oscillation events reported in the literature (Wang et al. 2003; Mariska 2006; Mariska et al. 2008), selecting only the events with a reported velocity amplitude, 93 events altogether. In addition, we included the event described by Kim et al. (2012), in which determining the relative amplitude of the density perturbation is possible. Using it, we estimated the relative velocity perturbation by taking that in an acoustic wave the relative density perturbation is equal to the ratio of the velocity perturbation to the sound speed. We also consider sloshing oscillations with the reported parameters taken from Kumar et al. (2013, 2015), Wang et al. (2015), Mandal et al. (2016), and Pant et al. (2017). This statistic includes observations of slow oscillations at approximately eight different temperatures, i.e., 14 MK and 12 MK with BCS, 13 MK, 10 MK, 7 MK, and 0.6 MK with AIA, 8.9 MK and 6.3 MK with SUMER, and 2 MK with EIS, using the estimations found in the papers mentioned above. In

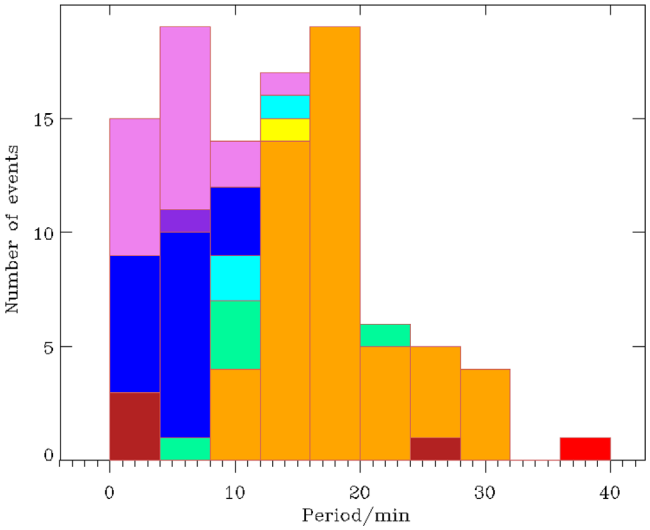

Figure 1. Distribution of the slow oscillation periods for different detection temperatures. The violet color corresponds to the temperature of 14 MK, magenta to 13 MK, blue to 12 MK, cyan to 10 MK, green to 8.9 MK, yellow to 7 MK, orange to 6.3 MK, red to 2 MK, and brick to 0.6 MK.

all cases, we neglected finite-β effects, estimating the slow wave speed as $152 \times (T[\mathrm{MK}])^{1/2}\,\mathrm{km\,s^{-1}}$.

Figure 1 shows the distribution of the detected periods of both SUMER and sloshing oscillations, with different colors corresponding to the temperatures associated with the emission lines or bandpasses used in the detections. The applied color scheme corresponds to a rainbow, i.e., the violet color represents the highest temperature, and the brick color the lowest temperature. It is evident that the detections in the hotter channels correspond to systematically shorter oscillation periods.

Figure 2 shows the scaling of the damping time with the oscillation period and the plasma temperature. It is clear that the decay time is apparently proportional linearly to the oscillation period. The scaling of the decay time τ_D with the period P was obtained by fitting a functional form $\tau_D = CP^p$, where C and p are constant, into the observational data, using Bayesian inference and Markov chain Monte Carlo (MCMC) sampling (see Pascoe et al. 2017, for the description of the method). The best fitting values are found to be $C = 1.18 \pm 0.4$ and $p = 0.87 \pm 0.1$, where uncertainties are estimated at the half levels of the Gaussian functions best-fitting the corresponding marginal posterior distributions. We need to point out that the marginal posterior distribution of the parameter C shows some deviations from the Gaussian shape, but it should not strongly affect the estimations. Thus, the results obtained with the extended data set, including results obtained with XRT, NoRH, and AIA are roughly consistent with the results obtained previously with SUMER (Verwichte et al. 2008) and with SUMER and BCS (Wang 2011), and also in soft X-rays in solar and stellar flares observed with *RHESSI* and *XMM-Newton* (Cho et al. 2016). Our value of the exponent, 0.87 ± 0.1, is close to unity. The large scattering of the data points does not allow one to determine whether this scaling depends on the specific value of the temperature.

We determined the oscillation Q-factor as the ratio of the damping time to the oscillation period, $Q = \tau_D/P$, i.e., the number of oscillation cycles detected in the event. From the fitting shown in Figure 2, the Q-factor is seen to weakly depend upon the oscillation period, so that taking the power-law index $p \approx 1$, the value of C could be considered as an average Q-factor of the detected slow oscillations. Sloshing oscillations are not significantly off the data cloud in this figure, and hence their damping mechanism could be similar to this of SUMER oscillations.

In Figure 3(a) we plot the Q-factor dependence on the apparent amplitude A, measured in the sound speeds corresponding to the temperature. In the case of the estimations by the Doppler shift, the amplitude is affected by the projection effect, and hence one should consider the top-right boundary of the data cloud in the figure as the actual scaling of the Q-factor

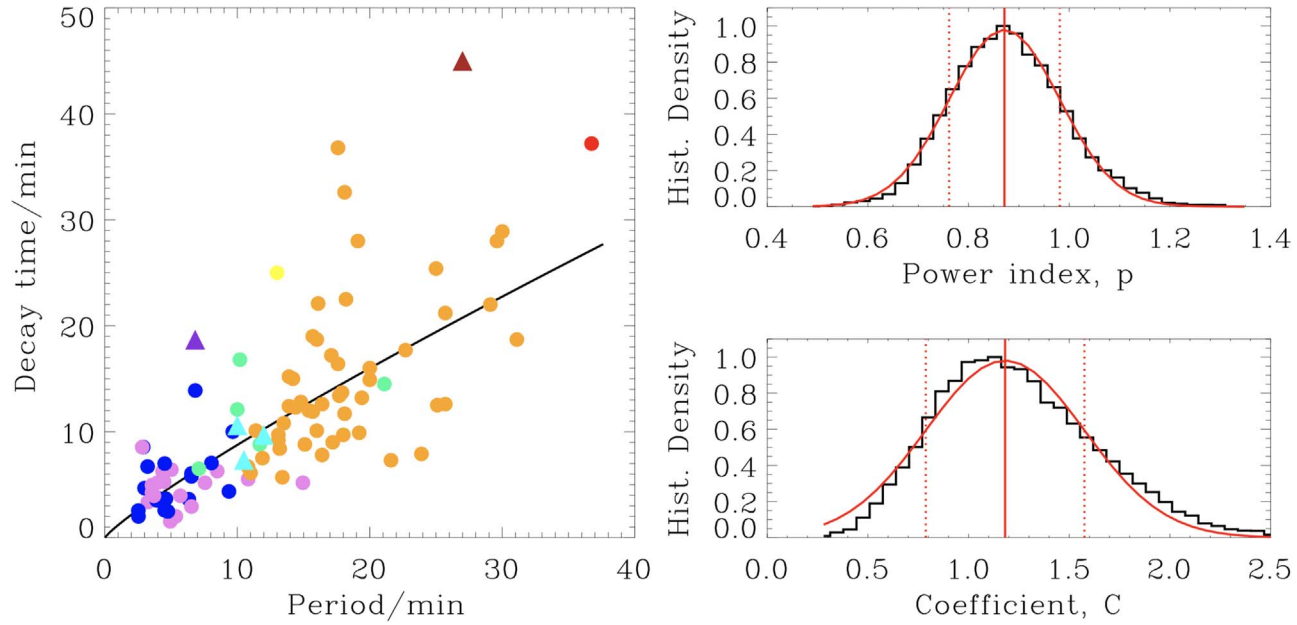

Figure 2. Left panel: scaling of the damping time of slow oscillations with the period. The colors represent different temperatures as described in Figure 1. The circles show SUMER oscillations; and triangles show sloshing oscillations. The black line indicates the best-fitting power law. Right panels: marginal posterior distributions for the model parameters p and C, obtained using Bayesian inference and MCMC sampling method. Red solid lines show the approximation of the corresponding distributions by the Gaussian function with the mean value (the vertical solid lines) and the half-level uncertainties (the vertical dotted lines).

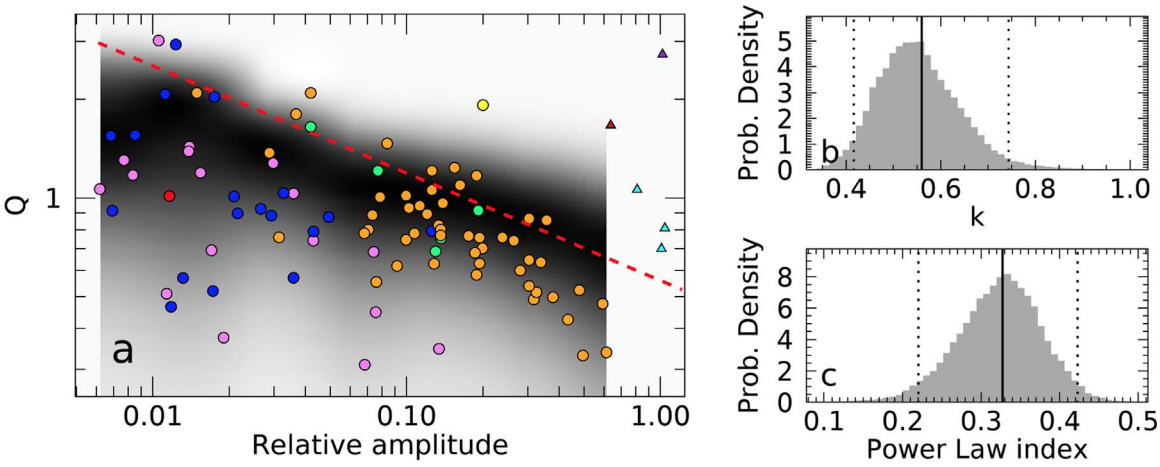

Figure 3. Scaling of the Q-factor vs. apparent relative amplitude (a). The data point legend is the same as those in Figures 1 and 2. The red dashed line shows the power-law dependence of the Q-factor upon the deprojected amplitude inferred using Bayesian analysis. The background color shows the posterior predictive probability distribution, which highlights areas where data points could be observed according to our model. Panels (b) and (c) show marginal posterior distributions for the normalization constant k and power-law index α.

with amplitude. A similar technique has been used for the demonstration of the nonlinear nature of kink oscillation damping by Goddard & Nakariakov (2016). The data cloud of slow oscillations in the figure clearly has a triangular shape, which indicates the dependence of the Q-factor on the amplitude, i.e., the nonlinear nature of the damping. We approximated the top-right boundary of the data cloud in a logarithmic scale by a linear function. In some cases, the relative amplitude could have an additional error caused by the neglect of the finite-β effect, i.e., the amplitude should be measured not in the units of the sound speed, but of the tube speed. However, this error is not likely to change the determined scaling qualitatively.

For accurate fitting of the Q-factor dependence upon the apparent amplitude, we use the following model,

$$Q_i = (k \cos\theta_i) A_i^{-\alpha} + N_i(0, \sigma), \quad (1)$$

where Q_i and A_i are the measured Q-factor and relative amplitude for the data point i, and α is the power-law index. The free parameter $N_i(0, \sigma)$ is a normally distributed random "noise" with a standard deviation σ, which represents scattering due to the measurement errors and possible dependence upon other properties of the loops. The projection effect is accounted for by the viewing angle θ_i as a free parameter. Bayesian inference based on this model revealed that $k = 0.56^{+0.18}_{-0.14}$ and $\alpha = 0.33^{+0.10}_{-0.11} \approx 1/3$ with 95% confidence. The marginal posterior distributions for k and α are shown in Figures 3(b) and (c). The shaded area in Figure 3(a) shows the predictive posterior distribution that demonstrates where the data points could be observed according to our model. Since the true deprojected amplitude (red dashed curve in Figure 3) corresponds to $\cos\theta = 1$, observed apparent amplitudes are expected to lie mostly below the curve as we see in our data set.

In Figure 3, we also show sloshing oscillations. Instead of the relative amplitude, for sloshing oscillations we used their projected phase speed determined by imaging observations. This is done in order to check whether the evolution of the sloshing blob is indeed produced by the slow wave phase or group speed, or should be attributed to a bulk flow, as the flows in the SUMER oscillations. The sloshing oscillations (shown by the triangles) are clearly off the data cloud in the figure, indicating that their apparent amplitude corresponds to the sound (tube) speed, and not the plasma flow speed. Also, it suggests that those slow oscillations that are in the data cloud (the circles), even if their nature was not identified observationally, e.g., because of the lack of the spatial information, are likely to be of the SUMER type, as has been previously assumed (e.g., Wang 2011).

3. Evolution of Different Spatial Harmonics

Figure 4 shows the evolution of the Fourier amplitudes of the four lowest spatial harmonics in the sloshing pulse of the EUV emission intensity in the event that occurred on 2012 May 7 (Kumar et al. 2013), determined by the cosine Fourier transform after the subtraction of the mean value from the intensity profile along the loop. The choice of the basis functions is dictated by the spatial structure of the density (intensity) perturbations in a standing slow wave. From the analysis, it is evident that the amplitudes of different harmonics of the sloshing disturbance evolve rather similarly, which indicates that they decay approximately at the same rate, independent of their wavelengths. Such a behavior is in apparent contradiction with the results shown in Figure 2, suggesting the need to account for both the competing effects of wavelength (or period) and nonlinearity on the damping.

4. Discussion and Conclusions

We performed statistical analysis of slow magnetoacoustic oscillations of coronal loops, based on the detections described in the literature, made in the EUV, SXR, and microwave bands, corresponding to the plasma temperatures from 0.6 to 14 MK. Thus, this study extends the statistical results determined previously for four temperatures by adding five new temperatures. Both standing and sloshing oscillations were considered. It was established that the oscillation period increases with the decrease in the temperature. Previously, this tendency determined by the SUMER and BCS data only, was attributed to the selection effect, as the oscillating loops observed at lower temperatures by SUMER are usually longer (Wang 2011). However, the detections made with AIA, NoRH, and XRT seem to correspond to the same pattern: oscillations seen in a

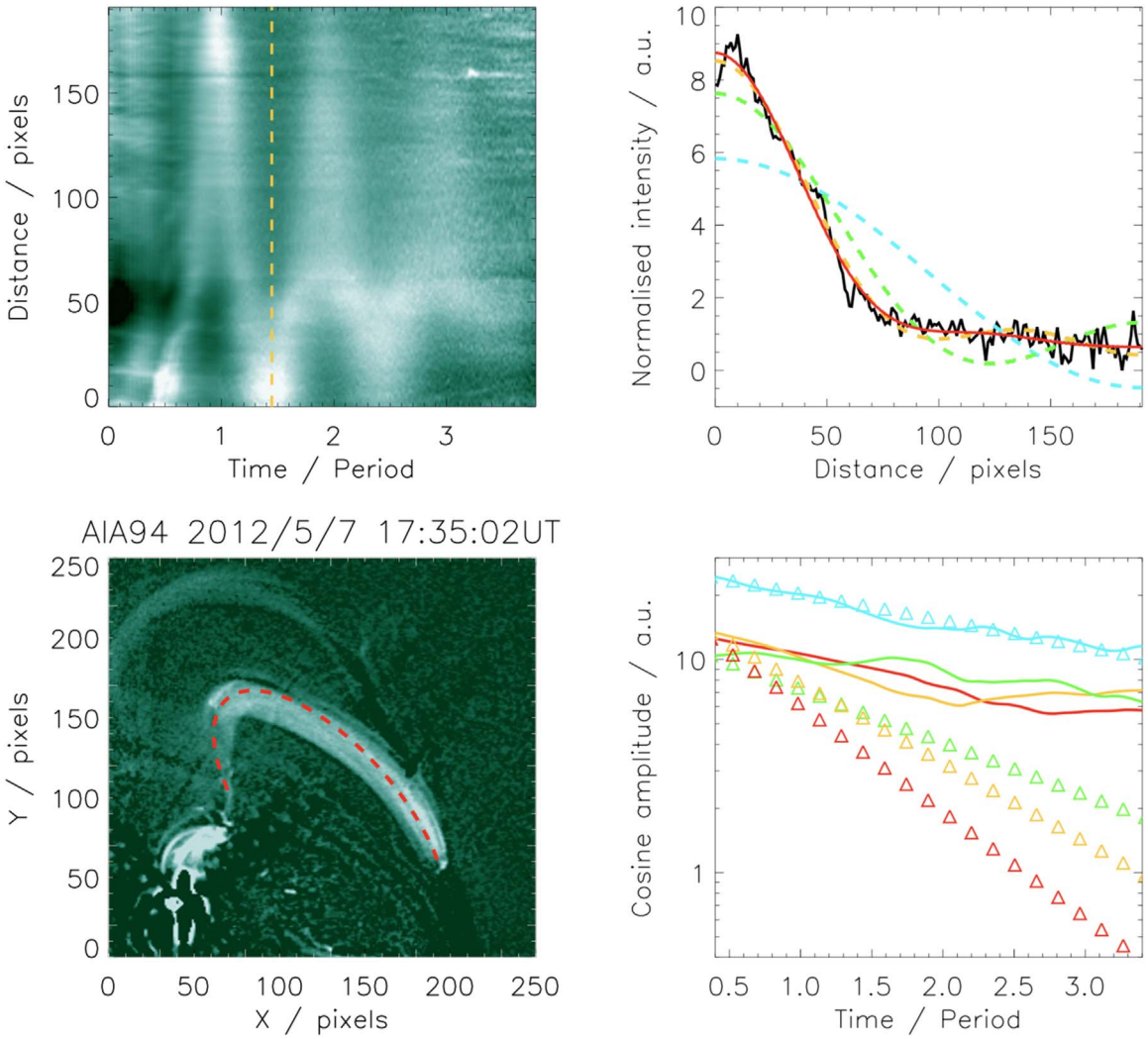

Figure 4. Top left: time–distance plot made for the slit along the loop shown in the bottom left panel. In each instant of time, the emission intensity is normalized to the mean value over the spatial coordinate. For each pixel, the mean value of the signal over time is subtracted. The time is measured in the units of the detected oscillation period, 630 s. The dashed vertical line indicates a certain instant of time in which the signal shown in the top right panel was taken. Bottom left: a snapshot on a sloshing oscillating loop observed by *SDO*/AIA at 94 Å. The red dashed line shows the elliptical slit along which the time–distance plot was made. Top right: a snapshot of the variation of the emission intensity along the loop (the black line). The light blue, green, yellow, and red lines show the lowest (fundamental) spatial harmonic, and summations of two lowest, three lowest, and four lowest harmonics, respectively. Bottom right: variation of the amplitude of the four lowest harmonics with time (solid lines). The blue, green, yellow, and red colors indicate the individual four lowest harmonics, respectively. The curves are smoothed with a running average over three oscillation periods. The triangles show the exponential dependence of the amplitudes of the corresponding individual harmonics upon time with the decay time being proportional to the harmonic number, i.e., to the oscillation period.

hotter plasma have shorter periods, with a few exceptions. Moreover, the newly discovered sloshing oscillations are consistent with this picture too. This behavior could be attributed to the decrease in the acoustic travel time with the increase in the temperature, i.e., in the sound speed.

All considered oscillation events, including sloshing, are consistent with the linear scaling of the damping time with the oscillation period, established for SUMER and BCS (Wang 2011). More rigorously, the use of the MCMC technique gives that the damping timescales with the oscillation period of 0.87 ± 0.1 at the half-level of a Gaussian fit, with the Q-factor being approximately constant at about unity. The insufficient number of observed events did not allow us to test this scaling for the sloshing oscillations only.

It was recently proposed that the linear scaling of the damping time and period could be attributed to the combined effect of anomalously large compressive viscosity and the Rosner–Tucker–Vaiana scaling (Wang et al. 2018). This suggests that oscillations of shorter wavelengths should decay faster. However, spatially resolved sloshing oscillations do not show a dispersion of the oscillating pulse. In other words, in the sloshing oscillations, the oscillating pulse remains localized along the loop, and there is no evidence of the preferential damping of the higher spatial spectral harmonics. Similar behavior is shown by full-scale numerical modeling (Reale 2016) and needs to be understood. This effect was tested by considering the time evolution of different spatial harmonics of a sloshing oscillation observed with AIA. It was discovered that four lowest harmonics show similar decay patterns. This may indicate that the enhanced damping of shorter harmonics is counteracted by another mechanism, e.g., nonlinearity. In particular, it could be explained by the competition of the dissipative processes, which tend to preferentially damp the shorter spatial harmonics, and the nonlinearity that leads to the preferential damping of the

harmonics with higher amplitudes and the nonlinear cascade to the higher harmonics.

The oscillation Q-factor is found to decrease with the relative amplitude (normalized to the sound speed), indicating the nonlinear nature of the damping. For the oscillations detected with SUMER, Verwichte et al. (2008) established that the inverse Q-factor depends linearly on the amplitude (see, also Ruderman 2013, who proposed the quadratic dependence). But, the line-of-sight projection effect was not taken into account in that study. Our finding, based on the Bayesian statistics shows that the Q-factor is proportional to the normalized relative amplitude to the power of $0.33^{+0.10}_{-0.11}$ with 95% confidence. The physical mechanism responsible for this effect needs to be identified.

This work was supported by STFC consolidated grant ST/P000320/1 (V.M.N. and D.Y.K.), the BK21 plus program through the National Research Foundation funded by the Ministry of Education of Korea (V.M.N. and Y.J.M.), the British Council Institutional Links Programme (M.K.K.), and the Russian Science Foundation under project No. 18-72-00144 (S.A.A.)

ORCID iDs

V. M. Nakariakov https://orcid.org/0000-0001-6423-8286
D. Y. Kolotkov https://orcid.org/0000-0002-0687-6172
S. A. Anfinogentov https://orcid.org/0000-0002-1107-7420
P. Kumar https://orcid.org/0000-0001-6289-7341
Y.-J. Moon https://orcid.org/0000-0001-6216-6944

References

Cho, I.-H., Cho, K.-S., Nakariakov, V. M., Kim, S., & Kumar, P. 2016, ApJ, 830, 110
de Moortel, I. 2009, SSRv, 149, 65
Fang, X., Yuan, D., Van Doorsselaere, T., Keppens, R., & Xia, C. 2015, ApJ, 813, 33
Goddard, C. R., & Nakariakov, V. M. 2016, A&A, 590, L5
Kim, S., Nakariakov, V. M., & Shibasaki, K. 2012, ApJL, 756, L36
Kolotkov, D. Y., Pugh, C. E., Broomhall, A.-M., & Nakariakov, V. M. 2018, ApJL, 858, L3
Kumar, P., Innes, D. E., & Inhester, B. 2013, ApJL, 779, L7
Kumar, P., Nakariakov, V. M., & Cho, K.-S. 2015, ApJ, 804, 4
Kumar, S., Nakariakov, V. M., & Moon, Y.-J. 2016, ApJ, 824, 8
Kupriyanova, E. G., Melnikov, V. F., Puzynya, V. M., Shibasaki, K., & Ji, H. S. 2014, ARep, 58, 573
Kupriyanova, E. G., & Ratcliffe, H. 2016, AdSpR, 57, 1456
Li, D., Ning, Z. J., Huang, Y., et al. 2017, ApJ, 849, 113
Mandal, S., Yuan, D., Fang, X., et al. 2016, ApJ, 828, 72
Mariska, J. T. 2005, ApJL, 620, L67
Mariska, J. T. 2006, ApJ, 639, 484
Mariska, J. T., Warren, H. P., Williams, D. R., & Watanabe, T. 2008, ApJL, 681, L41
McLaughlin, J. A., Nakariakov, V. M., Dominique, M., Jelínek, P., & Takasao, S. 2018, SSRv, 214, 45
Nakariakov, V. M., Afanasyev, A. N., Kumar, S., & Moon, Y.-J. 2017, ApJ, 849, 62
Nakariakov, V. M., Tsiklauri, D., Kelly, A., Arber, T. D., & Aschwanden, M. J. 2004, A&A, 414, L25
Nakariakov, V. M., & Zimovets, I. V. 2011, ApJL, 730, L27
Ofman, L., & Wang, T. 2002, ApJL, 580, L85
Ogrodowczyk, R., Murawski, K., & Solanki, S. K. 2009, A&A, 495, 313
Pant, V., Tiwari, A., Yuan, D., & Banerjee, D. 2017, ApJL, 847, L5
Pascoe, D. J., Anfinogentov, S., Nisticò, G., Goddard, C. R., & Nakariakov, V. M. 2017, A&A, 600, A78
Reale, F. 2016, ApJL, 826, L20
Reale, F., Lopez-Santiago, J., Flaccomio, E., Petralia, A., & Sciortino, S. 2018, ApJ, 856, 51
Reznikova, V. E., & Shibasaki, K. 2011, A&A, 525, A112
Ruderman, M. S. 2013, A&A, 553, A23
Selwa, M., Ofman, L., & Murawski, K. 2007, ApJL, 668, L83
Srivastava, A. K., & Dwivedi, B. N. 2010, NewA, 15, 8
Taroyan, Y., Erdélyi, R., Doyle, J. G., & Bradshaw, S. J. 2005, A&A, 438, 713
Tsiklauri, D., Nakariakov, V. M., Arber, T. D., & Aschwanden, M. J. 2004, A&A, 422, 351
Van Doorsselaere, T., Kupriyanova, E. G., & Yuan, D. 2016, SoPh, 291, 3143
Verwichte, E., Haynes, M., Arber, T. D., & Brady, C. S. 2008, ApJ, 685, 1286
Wang, T. 2011, SSRv, 158, 397
Wang, T., Innes, D. E., & Qiu, J. 2007, ApJ, 656, 598
Wang, T., Ofman, L., Sun, X., Provornikova, E., & Davila, J. M. 2015, ApJL, 811, L13
Wang, T., Ofman, L., Sun, X., Solanki, S. K., & Davila, J. M. 2018, ApJ, 860, 107
Wang, T., Solanki, S. K., Curdt, W., Innes, D. E., & Dammasch, I. E. 2002, ApJL, 574, L101
Wang, T. J., Solanki, S. K., Curdt, W., et al. 2003, A&A, 406, 1105
Yuan, D., Van Doorsselaere, T., Banerjee, D., & Antolin, P. 2015, ApJ, 807, 98